Available online at www.sciencedirect.com
ScienceDirect
Journal of the European Ceramic Society 30 (2010) 3181–3186
www.elsevier.com/locate/jeurceramsoc

In situ observation of the dissolution phenomena of SiC particle in $CaO–SiO_2–MnO$ slag

Joo Hyun Park [a,*], Jin Gyun Park [b], Dong Joon Min [b], Young E. Lee [c], Youn-Bae Kang [d]

[a] *School of Materials Science and Engineering, University of Ulsan, Moogeo-dong, Nam-gu, Ulsan 680-749, Republic of Korea*
[b] *Department of Materials Science and Engineering, Yonsei University, Seoul 120-749, Republic of Korea*
[c] *Metallic Materials Research Institute, Dongbu Metal, Donghae 240-143, Republic of Korea*
[d] *Graduate Institute of Ferrous Technology, POSTECH, Pohang 790-784, Republic of Korea*

Received 28 March 2010; received in revised form 24 June 2010; accepted 9 July 2010
Available online 4 August 2010

Abstract

The dissolution of SiC particle at 1600 °C in the $CaO–SiO_2–MnO$ slag was observed *in situ* by means of confocal scanning laser microscopy in order to make the determination of dissolution mechanism. The SiC particle is initially wetted by molten slag from the outer surface and the wetting between SiC and slag phase is more dominant in the composition of higher CaO/SiO_2 ratio. When the SiC particle is wetted by molten slag, the gas bubbles that are mainly CO gas is generated by the reaction between SiC and MnO in slag phase and are continuously evolved at the wetted area, which is pronounced as the CaO/SiO_2 ratio increases. The dissolution of SiC particle in the slag through the reaction with MnO is enhanced in the composition of higher CaO/SiO_2 ratio not only due to greater thermodynamic driving force but also due to accelerated mass transport kinetics.

Keywords: Interfaces; Corrosion; SiC; Refractories; Confocal scanning laser microscopy

1. Introduction

Interfacial reaction between carbide and molten slag phase is relevant for refractory life in the industrial fields including glass melting furnace and blast furnace.[1–6] There are some traditional ideas for the dissolution, *i.e*. local corrosion of clay-bonded carbide refractory into the slag due to an accelerated mass transfer caused by the Marangoni flow in an interfacial reaction film.[7] If the iron oxide were contained in slag phase, the SiC granules in the refractory were oxidized, which may facilitate the abrasion of the refractory.[8,9] Carbon/slag interactions have also been investigated between metallurgical coke (18.3 wt.% ash) and an EAF slag (35 wt.% Fe_2O_3) using a sessile drop arrangement.[10] There were significant carbon/slag interactions with the system exhibiting rapid iron oxide reduction and very high rates of gas generation. High level of gas generation led to a strong likelihood of convective transport of reactants and products across the coke/slag interface with oxides present in coke ash partially dissolving in slag.

Recently, in the production of silicomanganese (SiMn) alloys used for the alloying of various kinds of steels, the SiMn melt is saturated by SiC phase under condition of high silicon and low carbon concentration.[11] It has been believed that SiC particles are nucleated and grown in the SiMn melt and transported to the metal/slag interface. Finally, SiC particles might dissolve into the calcium silicate slag containing MnO of which content is from 10 to 30 wt.%. However, there is no experimental observation for the dissolution phenomena of SiC particles into the MnO-containing slag at high temperatures.

A high temperature confocal scanning laser microscopy (CSLM), combined with an infrared image furnace, allows for *in situ* observation of the dissolution behavior of microparticles in a slag. CSLM work has been carried out on the dissolution phenomena of MgO, Al_2O_3 and $MgAl_2O_4$ microparticles in the $CaO–SiO_2–Al_2O_3$ (–MgO) slags.[12–16] Consequently, in the present study, the dissolution of SiC particle at 1600 °C in the $CaO–SiO_2–MnO$ slag is observed *in situ* by means of CSLM and analyzed in order to make the determination of dissolution

* Corresponding author. Tel.: +82 52 259 2227; fax: +82 52 259 1688.
E-mail address: basicity@mail.ulsan.ac.kr (J.H. Park).

0955-2219/$ – see front matter © 2010 Elsevier Ltd. All rights reserved.
doi:10.1016/j.jeurceramsoc.2010.07.020

mechanism, which has not been clarified yet, more straightforward.

2. Experimental procedure

A confocal scanning laser microscope (CSLM) with a high temperature cell (Lasertec, VL2000DX) was used. In the CSLM, high-resolution images of material can be obtained that cannot be produced by most other conventional imaging techniques. Such imaging enables real time *in situ* observation of high temperature (up to 1700 °C) transient phenomena. The advantage of the CSLM technique with reference to traditional dissolution experiments using rods and cylinders is that the ratio of the volume of dissolving species to the volume of the solvent slag is very small.[16] Therefore, dissolution takes place without significant changes in the bulk composition of the slag. Details of the CSLM technique have been available elsewhere.[12–17]

The compositions of the slags used in this study are CaO–SiO_2–10 wt.% MnO (wt.% CaO/wt.% SiO_2 = C/S = 1.0) and CaO–SiO_2–20 wt.% MnO (C/S = 0.5). These systems are very important in a production of manganese alloys even though small amounts of Al_2O_3 and MgO are not included for the sake of simplification.[11] The slags were prepared by mixing the reagent-grade oxides and melting the mixture in a platinum crucible in a tube furnace under Ar at 1500 °C. After melting, the slag was quenched against a copper plate. A piece of quenched slag (~0.15 g) was then melted again in the CSLM before running an experiment. During an experiment, it is possible to follow the trajectory of the particle and keep focusing on it on the surface of the liquid slag.

The dissolution studies took place in a platinum crucible (4 mm in inner diameter and a height of 5 mm) by placing a piece of fused SiC (>99.9 wt.%) particle on the surface of a solid slag and heating this assembly to 1600 °C (Fig. 1) followed by holding for 30 min under an ultrahigh-purity flowing Ar atmosphere (200 ml/min). The Ar atmosphere was repeatedly switched to vacuum three times.

The thermal cycle during the dissolution experiment is of great importance and should allow the slag to melt before initiating the dissolution process. Therefore, in the present study, the sample was heated from an intermediate temperature, 1000 °C, at which the slag is solid and the dissolution rate is negligible, up to the desired experimental temperature, 1600 °C at a heating rate of 300 °C/min (Fig. 1). The sample temperature was measured by a B-type thermocouple welded on the bottom surface of the Pt holder containing the Pt crucible. The temperature accuracy was confirmed by melting experiments of pure copper (melting point: 1083 °C) and pure nickel (melting point: 1453 °C).

The video recordings of the dissolution process were analyzed to obtain the change in particle size with time. Because the shape of the initial SiC particle was not spherical but irregular plate-like, the largest diagonal distance of the particle was represented in this paper. The quenched sample was also observed by using SEM-EDS (Hitachi, S-4200).

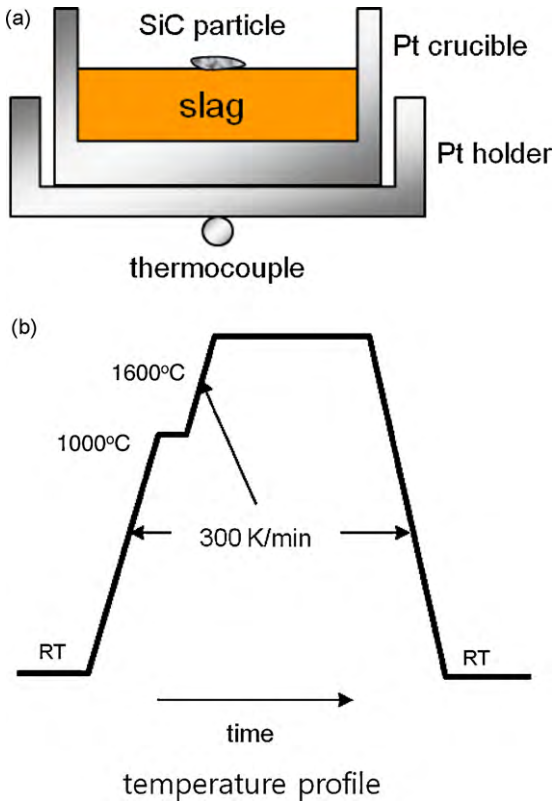

Fig. 1. A schematic of the sample and crucible configuration (a) and temperature profile during a CSLM experiment (b).

3. Results and discussion

The variations of morphology and size of SiC particles with reaction time are shown in Fig. 2(a) for the 45 wt.% CaO–45 wt.% SiO_2–10 wt.% MnO system (slag A) and Fig. 2(b) for the 27 wt.% CaO–53 wt.% SiO_2–20 wt.% MnO system (slag B) at 1600 °C. The SiC particles gradually shrink as the reaction time increases through the process of wetting by molten slags from the outer surface. As shown in Fig. 2(a), the wetting tendency by molten slag was more pronounced in case of the more basic system (slag A), where the outer surface of SiC particle was wetted by molten slag at very early stage and fully wetted by the slag at about 12 min at 1600 °C. However, the SiC particle was wetted by the relatively acidic (C/S = 0.5) silicate melt (slag B) at about 6 min later after reaching 1600 °C but not fully wetted by the slag through the entire holding time, *i.e.* 30 min in the present experiment as shown in Fig. 2(b). This is very interesting result which can be explained by the recent work by Safarian and Tangstad.[18] They measured the wettability of SiC single crystal substrate by liquid CaO–SiO_2 slags (C/S = 0.7–1.1) using a sessile drop technique and found that the wettability was relatively high for the basic slag. That is, the contact angle between slag and SiC substrate sharply decreased with increasing content of CaO. Even though the effect of MnO on the wettability between SiC and molten slag was not taken into account in their study, the present *in situ* observation results using CSLM shown in Fig. 1 are in good correspondence to the results measured by Safarian and Tangstad. Here, the density of

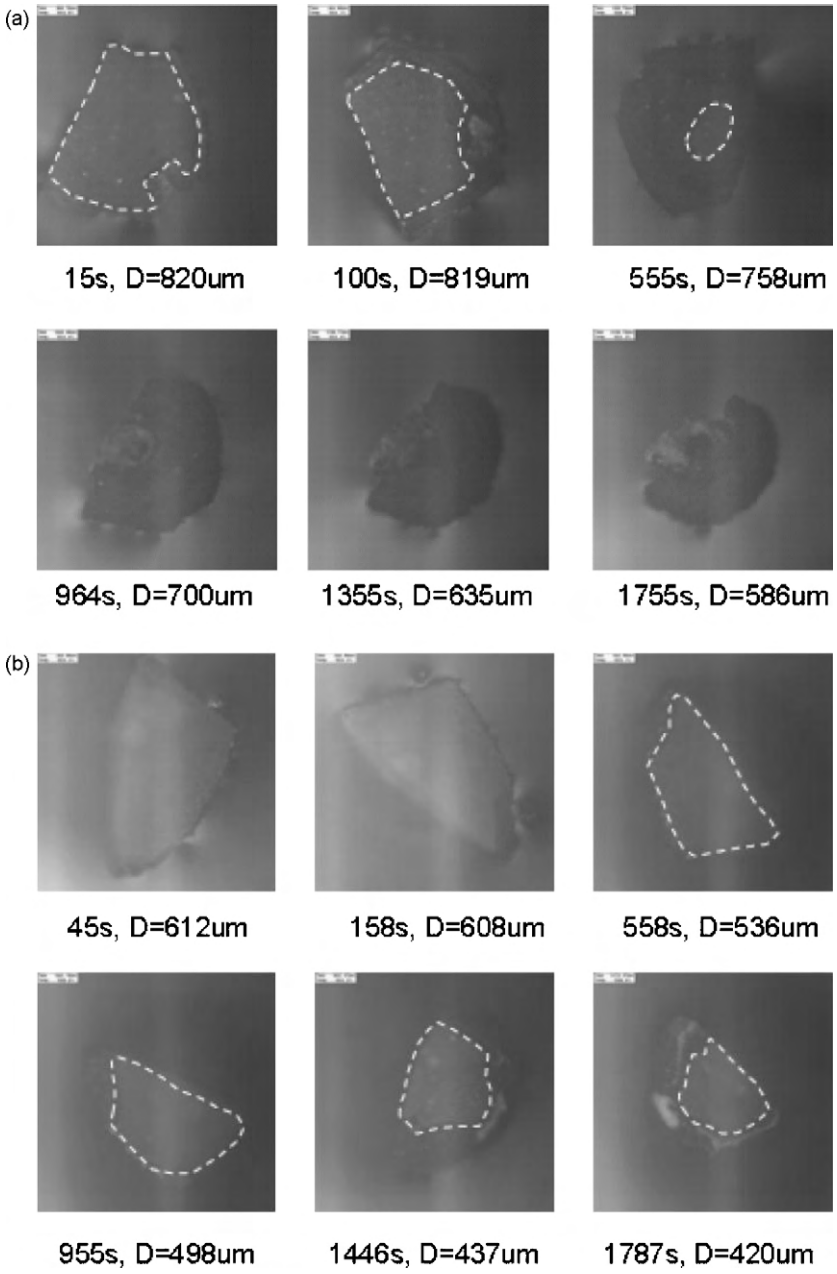

Fig. 2. Dissolution sequence of SiC particle in (a) CaO–SiO_2–10 wt.% MnO (C/S = 1.0; slag A) and (b) CaO–SiO_2–20 wt.% MnO (C/S = 0.5; slag B) slags at 1600 °C under a purified Ar atmosphere (unwetted area is the inner part of the dashed line).

slags A and B is relatively similar to each other, *viz*. about 2.7 and 2.8 g/cm^3, respectively, at 1500 °C.[19] Also, the shape of both particles is plate-like, even though the initial size is different. Hence, the difference in wettability of SiC and each slag system can be understood by employing the results by Safarian and Tangstad.

Furthermore, when the SiC particles dissolve into the slags, bubble bursting phenomena at the SiC/slag interface as well as at the wetted surface area of SiC particle was also observed as shown in Fig. 3(a). One can find small craters indicating the evolution of fine bubbles on the surface of SiC particle wetted by molten slag A (C/S = 1.0, 10 wt.% MnO) as shown in Fig. 2. Furthermore, the upper portion in Fig. 3(a) seems to get loose from main particle due to bubble bursting. However, as shown in Fig. 3(b), the surface of SiC particle reacted with slag B (C/S = 0.5, 20 wt.% MnO) is relatively clean, in which there is much less bubble bursting traces. Several possible reactions for the generation of gaseous species are as follows:[20]

$$3MnO + SiC = SiO_2 + 3Mn(g) + CO(g),$$
$$\Delta G^\circ = 963120 - 474T(J/mol) \quad (1)$$

$$MnO + SiC = SiO(g) + Mn(g) + C,$$
$$\Delta G^\circ = 605630 - 276T(J/mol) \quad (2)$$

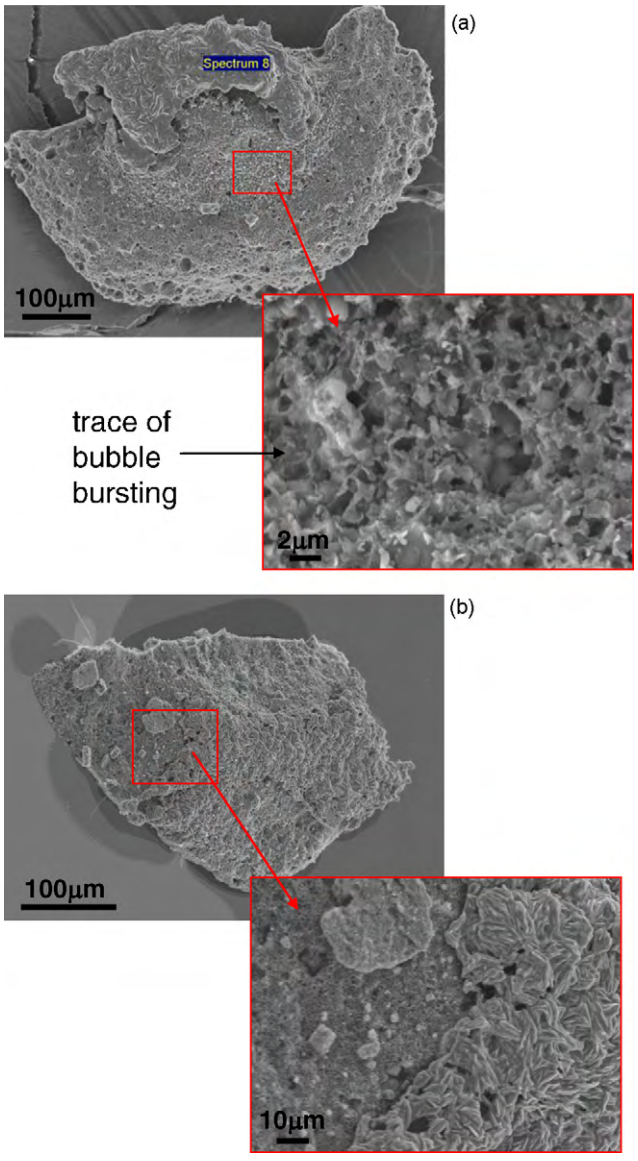

Fig. 3. Surface morphology of SiC particle reacted with (a) CaO–SiO_2–10 wt.% MnO (C/S = 1.0; slag A) and (b) CaO–SiO_2–20 wt.% MnO (C/S = 0.5; slag B) systems.

$$2SiO_2 + SiC = 3SiO(g) + CO(g),$$
$$\Delta G^\circ = 1457790 - 692T(J/mol) \quad (3)$$

However, because of very complicated characteristics of the present liquid–solid–gas systems, computational thermochemical software, FactSage™6.1 was employed to calculate the equilibrium composition of slag and gas phases at 1600 °C.[21–24] Here, the *FToxid* and *Fact53* databases were used. This package and databases have been successfully employed to evaluate the slag/refractory interfacial reactions.[25–29] The calculated partial pressure of gaseous species is plotted against the concentration of MnO according to the C/S ratio in Fig. 4, where the gas phase of which partial pressure lower than 10^{-4} atm, *e.g.* CO_2 is neglected. It is noticed that CO gas is the most dominant species evolved irrespective of the C/S ratio of slag, whereas the

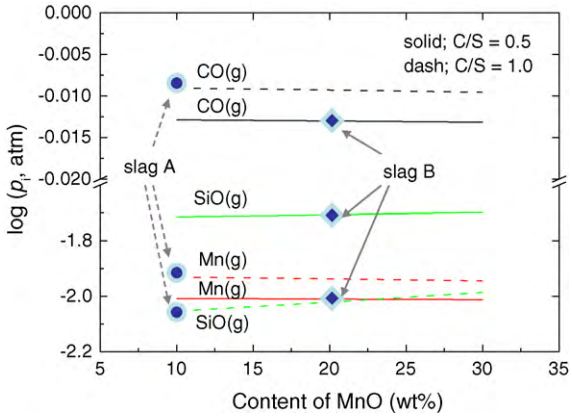

Fig. 4. The relationship between the equilibrium partial pressure of gaseous species with MnO content for C/S = 0.5 and 1.0, respectively.

partial pressure of SiO gas is strongly dependent of C/S ratio. The partial pressure of CO and Mn vapor in equilibrium with the more basic slag is greater than that with the acidic calcium silicate melt. Actually, as shown in Fig. 3, the bubble bursting phenomena was significantly observed when the SiC particle reacted with the basic melt (slag A). Thus, the calculated result is reasonably acceptable and shows a good correspondence to the experimental one.

The size of SiC particle is shown in Fig. 5 as a function of reaction time at 1600 °C. It seems that the apparent dissolution rate of the SiC particle into the slag A would be slightly faster than that into the slag B. Here, the slope of the line was obtained from a linear regression by least square method. This tendency can be qualitatively explained not only from the thermodynamics but also from the kinetics view as follows. First, as previously discussed, the reduction of MnO by SiC particle is energetically favorable at higher C/S ratio. Second, the greater the evolution of gas bubbles at higher C/S ratio, the faster the mass transport through the boundary layer is expected. Third, the viscosity of slag A (2 dPa s) is lower than that of slag B (5 dPa s) which was estimated by Ji (Fig. 6).[30] Even though the viscosity was evaluated at 1500 °C, the difference in the viscosity between slags A and B could be extrapolated to 1600 °C by

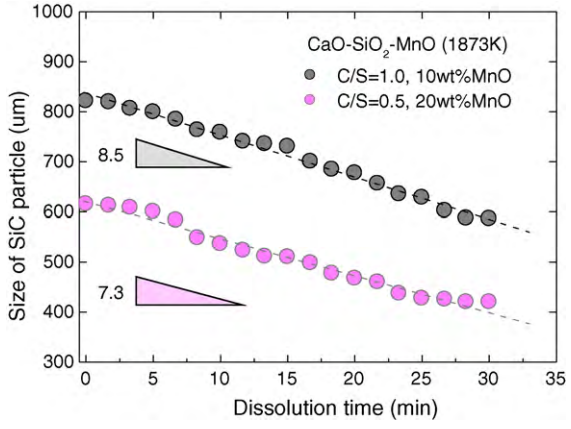

Fig. 5. Changes in the size of SiC particles dissolved into the CaO–SiO_2–MnO slag with reaction time at 1600 °C.

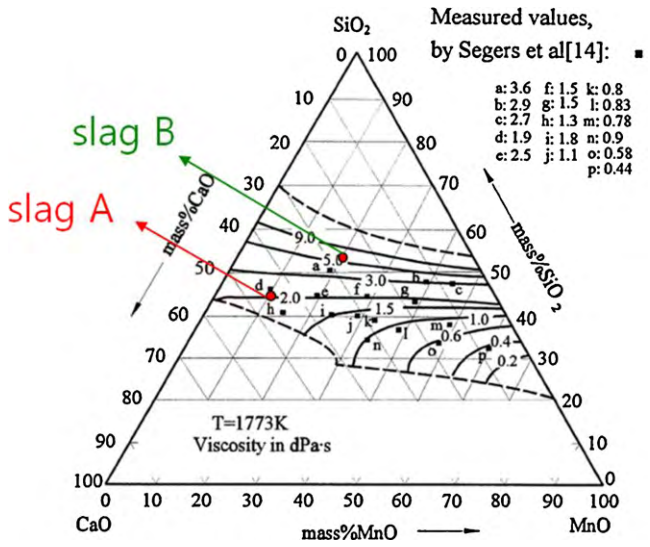

Fig. 6. Iso viscosity lines calculated by Ji in the CaO–SiO_2–MnO system at 1500 °C [modified from Ref. [29]].

assuming a Newtonian flow at high temperatures. Therefore, a dissolution reaction of SiC particle into the CaO–SiO_2–MnO slag is pronounced at high C/S ratio. However, because the duration of dissolution experiment at 1600 °C was limited to 30 min in the present study, the quantitative dissolution mechanism such as chemical or diffusion controls could not be obtained yet.[12–17,31] Thus, further works are needed to investigate the quantitative dissolution mechanism of SiC particle into the slag phase.

4. Conclusions

The dissolution of SiC particle at 1600 °C in the CaO–SiO_2–MnO slag is observed *in situ* by means of confocal scanning laser microscope and analyzed in order to make the determination of dissolution mechanism more straightforward. We may conclude that:

(1) The SiC particle is initially wetted by molten slag from the outer surface and the wetting between SiC and slag phase is more dominant in the composition of higher C/S ratio.
(2) When the SiC particle is wetted by molten slag, the gas bubbles that are mainly CO gas are continuously evolved at the wetted area, which is pronounced as the C/S ratio increases.
(3) The dissolution of SiC particle in the slag through the reaction with MnO is enhanced in the composition of higher CaO/SiO_2 ratio not only due to greater thermodynamic driving force but also due to accelerated mass transport kinetics.

References

1. Isola C, Salvo M, Ferraris M, Montorsi MA. Joining of surface modified carbon/carbon composites using a barium–aluminum–boro-silicate glass. *J Eur Ceram Soc* 1998;**18**:1017–24.
2. Zhang S, Marriott NJ, Lee WE. Thermochemistry and microstructures of MgO–C refractories containing various antioxidants. *J Eur Ceram Soc* 2001;**21**:1037–47.
3. Guo B-Y, Maldonaldo D, Zulli P, Yu A-B. CFD modeling of liquid metal flow and heat transfer in blast furnace hearth. *ISIJ Int* 2008;**48**: 1676–85.
4. Prompt N, Ouedraogo E. High temperature mechanical characterisation of an alumina refractory concrete for blast furnace main trough – part I. General context. *J Eur Ceram Soc* 2008;**28**:2859–65.
5. Inada T, Kasai A, Nakano K, Komatsu S, Ogawa A. Dissection investigation of blast furnace hearth – Kokura no. 2 blast furnace (2nd campaign). *ISIJ Int* 2009;**49**:470–8.
6. Zheng K, Wen Z, Liu X, Ren Y, Wu W, Qiu H. Research status and development trend of numerical simulation on blast furnace lining erosion. *ISIJ Int* 2009;**49**:1277–82.
7. Mukai K, Masuda T, Yoshitomi J, Harada T, Fujimoto S. Local corrosion of blast–furnace trough material at the slag surface. *Tetsu-to-Hagané* 1984;**70**:823–30.
8. Mukai K, Yoshitomi J, Harada T, Hurumi K, Fujimoto S. Local corrosion of blast furnace trough material at the slag–metal interface. *Tetsu-to-Hagané* 1984;**70**:541–8.
9. Yoshitomi J, Hiragushi K, Mukai K. The mechanism and the countermeasure of the local corrosion of blast furnace trough material at the slag–metal interface. *Tetsu-to-Hagané* 1987;**73**:1535–42.
10. Rahman M, Khanna R, Sahajwalla V, O'kane P. The influence of ash impurities on interfacial reactions between carbonaceous materials and eaf slag at 1550 °C. *ISIJ Int* 2009;**49**:329–36.
11. Olsen SE, Tangstad M, Lindstad T. *Production of manganese ferroalloys (chapter 4)*. Norway: SINTEF and Tapir Academic Press; 2007.
12. Valdez M, Prapakorn K, Cramb AW, Sridhar S. Dissolution of alumina particles in CaO–Al_2O_3–SiO_2–MgO slags. *Ironmak Steelmak* 2002;**29**: 47–52.
13. Monaghan BJ, Chen L. Effect of changing slag composition on spinel inclusion dissolution. *Ironmak Steelmak* 2006;**33**:323–30.
14. Valdez M, Shannon GS, Sridhar S. The ability of slags to absorb solid oxide inclusions. *ISIJ Int* 2006;**46**:450–7.
15. Liu J, Guo M, Jones PT, Verhaeghe F, Blanpain B, Wollants P. *In situ* observation of the direct and indirect dissolution of MgO particles in CaO–Al_2O_3–SiO_2 based slags. *J Eur Ceram Soc* 2007;**27**: 1961–72.
16. Liu J, Verhaeghe F, Guo M, Blanpain B, Wollants P. *In situ* observation of the dissolution of spherical alumina particles in CaO–Al_2O_3–SiO_2 melts. *J Am Ceram Soc* 2007;**90**:3818–24.
17. Jones PT, Desmet D, Guo M, Durinck D, Verhaeghe F, Dyck JV, et al. Using confocal scanning laser microscopy for the *in situ* study of high-temperature behaviour of complex ceramic materials. *J Eur Ceram Soc* 2007;**27**:3497–507.
18. Safarian J, Tangstad M. Wettability of silicon carbide by CaO–SiO_2 slags. *Metall Mater Trans B* 2009;**40B**:920–8.
19. Keene BJ, Mills KC. *Densities of molten slags, in slag atlas (chapter 8)*. 2nd ed. Dusseldorf, Germany: Verlag Stahleisen GmbH; 1995.
20. Turkdogan ET. *Physical chemistry of high temperature technology (chapter 1)*. New York, NY: Academic press; 1980.
21. www.factsage.com.
22. Kang YB, Jung IH, Decterov SA, Pelton AD, Lee HG. Critical thermodynamic evaluation and optimization of the CaO–MnO–SiO_2 and CaO–MnO–Al_2O_3 systems. *ISIJ Int* 2004;**44**:965–74.
23. Kang YB, Jung IH, Decterov SA, Pelton AD, Lee HG. Phase equilibria and thermodynamic properties of the CaO–MnO–Al_2O_3–SiO_2 system by critical evaluation, modeling and experiment. *ISIJ Int* 2004;**44**:975–83.
24. Bale C, Belisle E, Chartrand P, Decterov SA, Eriksson G, Hack K, et al. FactSage thermochemical software and databases – recent developments. *Calphad* 2009;**33**:295–311.
25. Park JH. Solidification behavior of calcium aluminosilicate melts containing magnesia and fluorspar. *J Am Ceram Soc* 2006;**89**:608–15.
26. Park JH. Formation of $CaZrO_3$ at the interface between CaO–SiO_2–MgO–CaF_2 (–ZrO_2) slags and magnesia refractories: computational and experimental study. *Calphad* 2007;**31**:149–54.

27. Park JH. Solidification structure of $CaO–SiO_2–MgO–Al_2O_3$ ($–CaF_2$) systems and computational phase equilibria: crystallization of $MgAl_2O_4$ spinel. *Calphad* 2007;**31**:428–37.
28. Suk MO, Park JH. Corrosion behavior of zirconia refractory by $CaO–SiO_2–MgO–CaF_2$ slag. *J Am Ceram Soc* 2009;**92**:717–23.
29. Park JH, Jung IH, Lee SB. Phase diagram study for the $CaO–SiO_2–Cr_2O_3$–5mass%MgO–10mass%MnO system. *Met Mater Int* 2009;**15**:677–81.
30. Ji FZ. Experimental studies of the viscosities in $CaO–MnO–SiO_2$ and $CaO–Fe_nO–MnO–SiO_2$ slags. *Metall Mater Trans B* 2001;**32B**: 181–6.
31. Levenspiel O. *Chemical reaction engineering (chapter 25)*. 3rd ed. New York, NY: John Wiley & Sons; 1999.